THE ASTROPHYSICAL JOURNAL SUPPLEMENT SERIES, 99:543–549, 1995 August

HUBBLE SPACE TELESCOPE IMAGES OF THE NUCLEAR STAR-FORMING REGION IN THE INTERACTING GALAXY NGC 5930[1]

GARY A. BOWER AND ANDREW S. WILSON[2]
Space Telescope Science Institute, 3700 San Martin Drive, Baltimore, MD 21218; bower@stsci.edu, awilson@stsci.edu
Received 1994 October 10; accepted 1995 February 6

ABSTRACT

High-resolution images of the spiral galaxy NGC 5930 have been obtained with the Planetary Camera aboard the *Hubble Space Telescope* in the emission lines of [O III] λλ4959, 5007 + Hβ and Hα + [N II] λλ6548, 6583, and their adjacent continua. NGC 5930 is the interacting companion of the Type 2 Seyfert galaxy NGC 5929. Five bright continuum knots, which probably represent star clusters, are found in the central $\simeq 1\farcs5$ ($200\ h^{-1}$ pc, $h = H_0/100$ km s^{-1} Mpc^{-1}). Four of these knots are associated with an elliptical ring of low-excitation gas with dimensions $2\farcs4 \times 1\farcs6$ ($320\ h^{-1} \times 220\ h^{-1}$ pc), while the fifth lies close to the ring's center. This gaseous ring, which probably lies in the plane of the disk, has an Hα luminosity $\approx 7 \times 10^{40}\ h^{-2}$ ergs s^{-1}. Assuming that the initial mass function for 5–120 $M_\odot$ stars is represented by a power law with an exponent of −2.5, the Hα luminosity implies a modest star formation rate of $0.07\ h^{-2}\ M_\odot$ yr^{-1} for 5–120 $M_\odot$ stars, and a supernova rate from the explosion of massive stars $\approx 3 \times 10^{-3}\ h^{-2}$ yr^{-1}. This nuclear star forming region appears to be similar to other nuclear rings in spiral galaxies. It has often been argued that such nuclear rings form at or near the inner Lindblad resonance. If this is the case for NGC 5930, the small radius of the ring implies a strongly concentrated central mass distribution.

Subject headings: galaxies: individual (NGC 5930)—galaxies: ISM—galaxies: nuclei—galaxies: starburst—galaxies: star clusters—galaxies: structure

1. INTRODUCTION

Recent theoretical work has shown that galaxy interactions can concentrate gas into the galactic nuclei. This process is sometimes associated with the formation of a stellar bar (e.g., Noguchi 1988; Mihos & Hernquist 1994), the nonaxisymmetric gravitational potential of which can force interstellar gas inward (e.g., Barnes & Hernquist 1991; Mihos, Richstone, & Bothun 1992). As gas settles toward the nucleus, it is expected to form a ring at or near the inner Lindblad resonance if such a resonance exists (e.g., Buta & Crocker 1993). Thus, some interacting galaxies may be expected to contain rings of ionized gas around their nuclei.

NGC 5930, a non-Seyfert spiral galaxy, and its companion NGC 5929, a Type 2 Seyfert galaxy, are listed in samples of interacting galaxies (e.g., Kennicutt et al. 1987) since the projected separation between the galaxy nuclei is only 28″ ($\approx 4\ h^{-1}$ kpc for a distance of $28\ h^{-1}$ Mpc, $h = H_0/100$ km s^{-1} Mpc^{-1}) and their redshifts differ by only 158 km s^{-1}. This interacting pair is also known as Arp 90. Previous ground-based observations have revealed that the nuclei of both galaxies contain ionized gas (Keel 1985; Keel et al. 1985). The ionized gas in the nucleus of NGC 5930 is of low excitation, and consistent with emission from H II regions. Wakamatsu & Mishida (1988) find that the gas extends over only $3\farcs6$ ($490\ h^{-1}$ pc), and exhibits two kinematic components separated by 197 km s^{-1}. This strong concentration of the nuclear gas in NGC 5930 may have resulted from its interaction with NGC 5929.

In order to determine the morphologies of the gas and stars in the nucleus of NGC 5930, we have obtained images of the galaxy with the *Hubble Space Telescope* (*HST*) in the optical emission lines [O III] λλ4959, 5007 + Hβ and Hα + [N II] λλ6548, 6583, and in their adjacent continua. The basic properties of NGC 5930, taken from de Vaucouleurs et al. (1991), except as noted, are given in Table 1. The galaxy was observed simultaneously with NGC 5929, the images of which have been presented elsewhere (Bower et al. 1994).

2. OBSERVATIONS AND REDUCTIONS

NGC 5930 was observed with *HST* on 1992 September 27 with the Planetary Camera (MacKenty et al. 1992). More details of these observations are given in Bower et al. (1994). Table 2 lists the effective wavelengths and bandpass widths of the filters, which were chosen to isolate the emission lines of Hβ + [O III] λλ4959, 5007 and Hα + [N II] λλ6548, 6583, and their adjacent continua. Keel et al. (1985) found [O III] λ5007/Hβ = 0.43 through a circular aperture $4\farcs7$ in diameter centered on the nucleus, so [O III] emission accounts for 36% of the total flux from emission lines in the F492M filter. Individual exposure times were typically 900 s, with two exposures obtained in each of the on-band filters (F492M and F664N) and one exposure in each of the off-band filters (F547M and F718M). The initial guide star acquisition was maintained throughout all exposures by tracking in fine lock. Data reduction was accomplished by following the procedure given in detail by Bower et al. (1994). NGC 5930's nuclear region was

[1] Based on observations with the NASA/ESA *Hubble Space Telescope*, obtained at the Space Telescope Science Institute, which is operated by the Association of Universities for Research in Astronomy, Inc., under NASA contract NAS5-26555.

[2] Also Astronomy Department, University of Maryland, College Park, MD 20742

TABLE 1

BASIC PROPERTIES OF NGC 5930

Property	Value
Optical Position (1950.0)[a]	$\alpha = 15^h24^m20^s.70$, $\delta = +41°51'00''.4$
Morphological Type	SAB(rs)b pec
Heliocentric Redshift	2672 km s^{-1}
Scale	135 h^{-1} pc arcsec^{-1}
B_0^T[b]	12.7
Major axis PA[c]	165°
b/a	0.52
Inclination[c]	46°
M_B[d]	−19.5
A_B[e]	0.06 mag

[a] Argyle & Clements 1990; formal estimated error is ±0".14 in each coordinate.
[b] Keel et al. 1985.
[c] Wakamatsu & Nishida 1988.
[d] $H_0 = 100$ km s^{-1} Mpc^{-1}.
[e] Galactic extinction toward NGC 5930 (Burstein & Heiles 1984).

detected with S/N ≈ 20–25 pixel^{-1}. The accuracy of flat-field calibration is ~5%, as indicated by the dispersion about the mean background sky level. Figure 1 shows the sum of the F547M and F718M continuum images *before* deconvolution; this figure is used in § 3 to examine the morphology of NGC 5930. As in Bower et al. (1994), each image was then deconvolved using 50 iterations of the Lucy (1974) algorithm, yielding resolution ≃0".1. All features in the deconvolved images are also apparent in the images before deconvolution, although with lower contrast. Since the effective wavelengths of the F547M and F718M filters are close to those of the Johnson V and R bandpasses, the observed continuum color may be converted to $(V-R)$ by

$$(V-R) = 2.5 \log [F_\lambda(7160\ \text{Å})/F_\lambda(5460\ \text{Å})] + 0.85, \quad (1)$$

where the zero point is from Allen (1973). A check on the flux calibration of the deconvolved images was accomplished by using the spectrum of Keel et al. (1985) to calculate a simulated flux through each *HST* filter. A comparison of the fluxes from these simulations with the actual *HST* fluxes is shown in Table 2. From the spectroscopy of Keel et al. (1985), we estimate that emission from [S II] λλ6717, 6731 accounts for ≈4% of the detected flux in the central 4".7 of the F718M image.

3. RESULTS

Since theoretical work suggests that galaxy interactions can lead to the formation of bars (§ 1), it is useful to examine the global morphology of NGC 5930. Although de Vaucouleurs et al. (1991) classify this galaxy as SAB(rs)b pec, no signs of a bar are apparent on the plates of Arp (1966) and the digitized sky survey obtained for the Guide Star Catalogue (Lasker et al. 1990). However, a barlike structure with P.A. ≈ 70° extending ≈6" (810 h^{-1} pc) from the nucleus is apparent in the *HST* continuum images (Fig. 1). *BVI* images obtained by M. Mateo with the Michigan Dartmouth MIT 2.4 m telescope confirm the presence of a bar with this size and position angle. As denoted by (rs) in de Vaucouleurs et al.'s classification, NGC 5930 contains a "pseudoring" (a term defined by Buta 1986), with diameter ≃ 17" × 25" = 2.3 h^{-1} × 3.3 h^{-1} kpc. These morphological features indicate the presence of a nonaxisymmetric gravitational potential.

Figure 2 and Figure 3 (Plate 9) show the deconvolved images. Five bright continuum knots are found in the central ≃1".5 (200 h^{-1} pc), so there is some uncertainty in the identification of the true nucleus. Fitting elliptical isophotes to the *HST* continuum images outside the central region (i.e., $R >$ 2") results in a position (with error ≈ ±0".2) for the photometric center consistent with a bright knot lying between the other four knots. We will refer to this position (marked by a cross in Figs. 2 and 3) as the "nucleus" while recognizing the ambiguity in relating this position to the mass center of the galaxy. The Hα + [N II] image shows that the ionized gas is concentrated into a ring, the center of which coincides with the nucleus, with a spur extending tangentially ~1" south of the nucleus. The bright continuum knots could either be star clusters or represent a smooth stellar distribution affected by patchy obscuration. Individual star clusters are known to exist in some galactic nuclei. For example, Benedict et al. (1993) published an *HST I* image of the spiral galaxy NGC 4314, resolving the central region into individual star clusters in a nuclear ring with a spiral pattern of discrete dust clouds. On the other hand, images from *HST* are revealing small (~100–500 pc) nuclear dust concentrations in some galaxies (e.g., Bower et al. 1994; Mulchaey et al. 1994; Grillmair et al. 1994). The ratio of the red and green continuum images (Fig. 4 [Pl. 10]) demonstrates that the region between the bright knots has approximately the same color ($V-R$ = 1.6 mag) as the stellar continuum at $R \geq 2$", suggesting that this region is not heavily reddened relative to the region at $R \geq 2$". Since the region between the bright continuum knots also exhibits diffuse Hα +

TABLE 2

BANDPASS FLUXES OF NGC 5930

Name	Filter λ_c (Å)	FWHM (Å)	*HST* Photometry (ergs cm^{-2} s^{-1})	Synthetic Photometry[a] (ergs cm^{-2} s^{-1})	Difference (%)
F492M	4915	364	6.88×10^{-13}	1.53×10^{-12}	−55
F547M	5461	438	9.39×10^{-13}	1.62×10^{-12}	−42
F664N	6637	131	6.42×10^{-13}	6.37×10^{-13}	0.8
F718M	7164	593	1.94×10^{-12}	1.54×10^{-12}	26

[a] Based on the Keel et al. 1985 ground-based spectrum (see text).

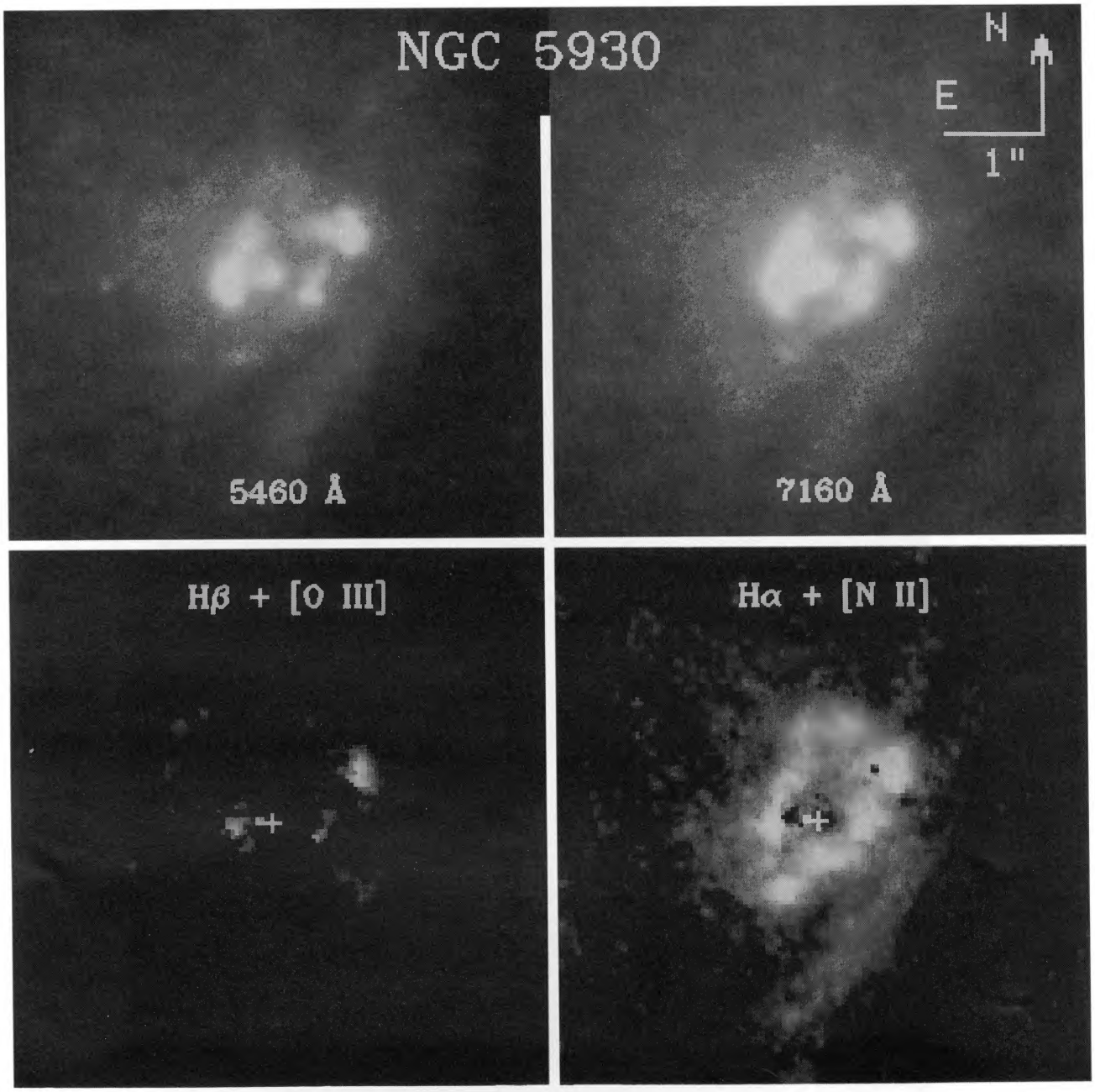

FIG. 3.—The deconvolved *HST* Planetary Camera images of the nuclear region of NGC 5930. The orientation is indicated by the bars, each of which is 1″ long. These deconvolved images have resolution of 0″.1. The continuum images (*upper panels*) were used to subtract the contribution of continuum light in the on-band images, producing the emission-line images (*lower panels*). The intensity scale is logarithmic with a range of 0 to 1.1×10^{-15} ergs cm^{-2} s^{-1} Å^{-1} arcsec^{-2} in the continuum images, 0 to 3.9×10^{-13} ergs cm^{-2} s^{-1} arcsec^{-2} in the Hβ + [O III] image, and 0 to 1.4×10^{-13} ergs cm^{-2} s^{-1} arcsec^{-2} in the Hα + [N II] image. The adopted position of the nucleus is marked by a cross in the lower panels.

BOWER & WILSON (see 99, 544)

PLATE 10

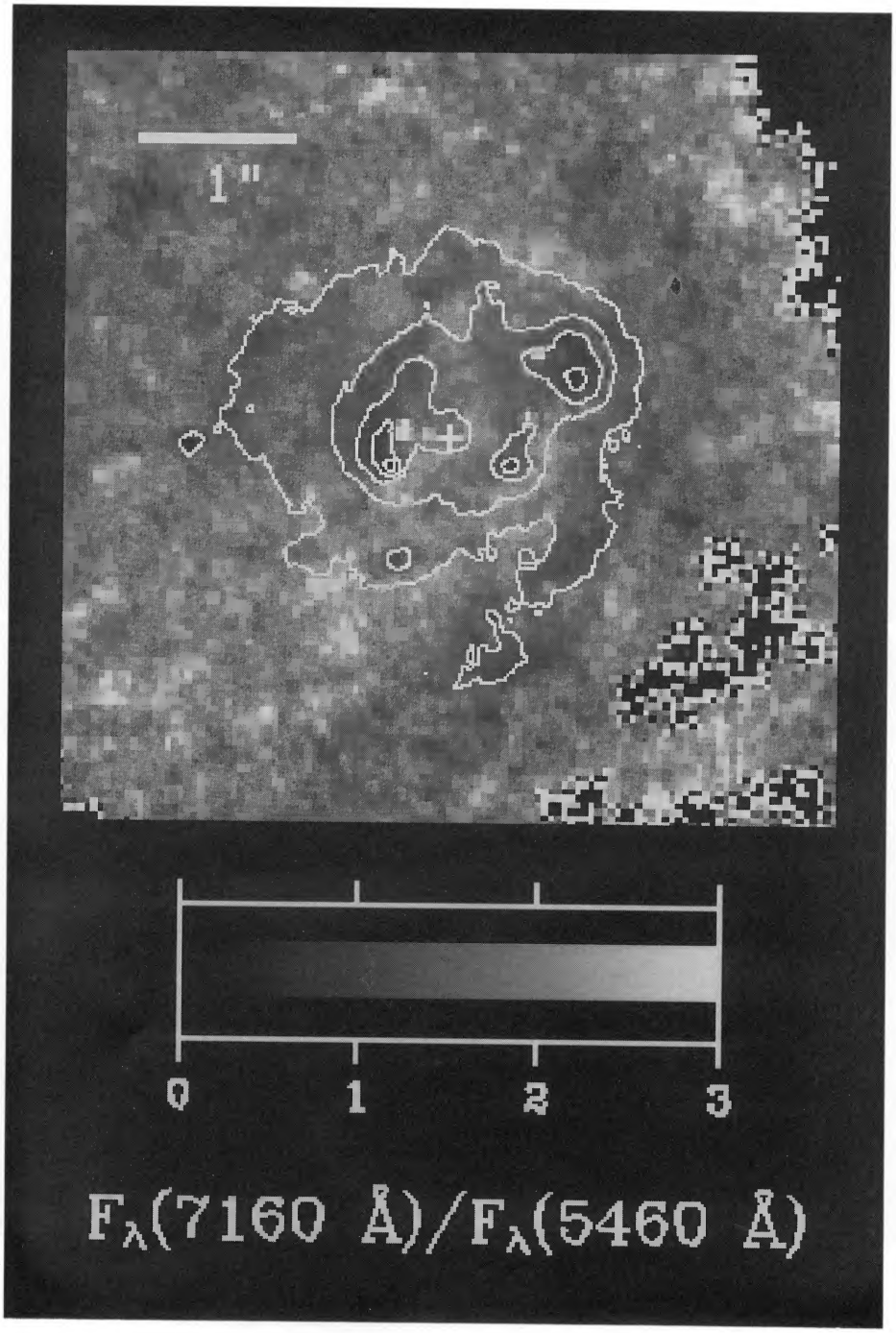

FIG. 4.—The ratio of the continuum images in Fig. 3 [F_λ(7160 Å)/F_λ(5460 Å)] is shown in gray scale with the green continuum contours superposed. North is up, and east is to the left. This color map was constructed so that the ratio was set to zero for those pixels with continuum surface brightness less than 5 σ above the background. All such pixels occurred outside the region of interest (i.e., $R \geq 2''$, in the upper and lower right portions of the color map). Lighter shades indicate redder continuum colors. The variation of the continuum color in the nuclear star forming region may be due to an excess of hotter stars in the star clusters compared to the mean stellar population or to variations in extinction. The ratio values are related to $(V-R)$ colors by $(V-R) = 2.5 \log [F_\lambda(7160\ \text{Å})/F_\lambda(5460\ \text{Å})] + 0.85$.

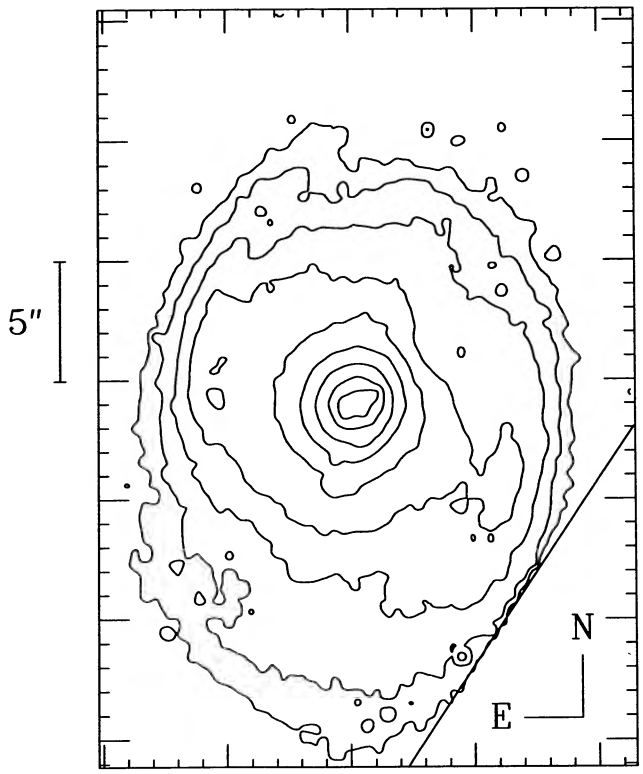

FIG. 1.—A contour plot of the sum of the F547M and F718M *HST* Planetary Camera images of NGC 5930 *before* deconvolution. The SW edge of the field of view is marked by the line running diagonally across the lower right corner. The contours were smoothed so that the effective resolution of this plot is $\simeq 1''$. The nine contours have intensities of 1.0%, 1.6%, 2.5%, 4.0%, 6.3%, 10%, 15%, 25%, and 39% of the peak intensity (163 counts pixel^{-1}). Thus the contour interval is 0.5 mag. This image shows a barlike structure with P.A. $\approx 70°$. The type 2 Seyfert galaxy NGC 5929 lies 28″ SW of NGC 5930.

[N II] emission (see below), it is unlikely that this region is heavily obscured, so the interpretation of the bright knots as star clusters is favored.

In order to estimate the rate of formation of massive stars from the Hα luminosity, an estimate of the extinction is needed. Keel et al. (1985) found an emission-line flux ratio corrected for underlying Balmer absorption of $F_{\rm obs}(\mathrm{H}\alpha)/F_{\rm obs}(\mathrm{H}\beta) = 10.9$ for the central 4″.7. Assuming the gas is optically thick to Lyman continuum photons (case B) and $T_e = 10^4$ K, the intrinsic emission-line decrement $F(\mathrm{H}\alpha)/F(\mathrm{H}\beta) = 2.86$. For the Galactic interstellar extinction curve (Savage & Mathis 1979), the visual and Hα extinctions are $A_V = 3.8$ mag and $A_{\mathrm{H}\alpha} = 2.9$ mag, respectively. It should be emphasized that this estimate of the extinction is an average over Keel et al.'s 4″.7 aperture, inside which the extinction could vary.

Table 3 lists the photometry of the five star clusters (A–E) and the nuclear region. This table provides the star cluster identification, the aperture diameter, the V magnitude, the absolute magnitude, M_V, for the cases of $A_V = 0$ and $A_V = 3.8$ mag, the observed continuum color $(V - R)$, the peak surface brightness $\mu_0(V)$, and the apparent core radius r_c (the radius at which the observed surface brightness is half of its peak value). Aperture sizes were chosen to be as large as possible without overlap for the five star clusters and to encompass the entire nuclear star forming region. The observed continuum color is a few percent too red at locations of bright ionized gas due to contamination of the F718M filter by [S II] emission (§ 2). With the exception of M_V, no corrections have been applied to the numbers in Table 3 for reddening. The contribution to the continuum emission from the ionized gas is small (e.g., Osterbrock 1989).

The elliptical ring, with dimensions 2″.4 × 1″.6 (320 h^{-1} × 220 h^{-1} pc), of Hα + [N II] emission (Figs. 2 and 3) has an axial ratio $b/a \approx 0.67$. Table 4 includes the luminosity in Hα + [N II]; applying corrections for the contribution of [N II] λλ6548, 6583 and the extinction yields an Hα luminosity $\approx 7 \times 10^{40}\ h^{-2}$ ergs s^{-1}. Thus the size and Hα luminosity are comparable to those of familiar giant H II regions in nearby galaxies, such as M101 (e.g., Kennicutt 1984). Apart from a few areas with no line emission, it appears that the interior of the ring contains faint diffuse Hα + [N II] emission. The major axis position angle of the emission-line ring is ≈140°, in agreement with the value of 150° ± 15° inferred by Wakamatsu & Nishida (1988). This ring probably lies in the plane of the galaxy disk, since the ring's axial ratio and major axis position angle are similar to those of the disk (Table 1). The emission-line ratios (Keel et al. 1985) indicate that the gas is ionized by hot stars, which may lie in the nuclear star clusters described above.

4. DISCUSSION

Having discussed the morphology of the nuclear star forming region in § 3, we now compare (§ 4.1) the supernova rate inferred from the extinction-corrected Hα luminosity with that from the nonthermal radio luminosity. We consider a possible mechanism for the formation of the nuclear star forming region in § 4.2.

4.1. *Star Formation Rate and Supernova Rate in the Nuclear Star Forming Region*

Stellar population synthesis models (e.g., Leitherer 1990) can be used to estimate the star formation rate (SFR) and supernova rate ($R_{\rm SN}$) in the nuclear star forming region in NGC 5930 from the ionizing luminosity as measured by the Hα luminosity. Leitherer's (1990) models (see his Table 3) provide estimates of the SFR for the mass range of 5–120 $M_\odot$ and $R_{\rm SN}$ normalized to ionizing luminosity for a range of initial mass functions (IMFs). Analysis of nine OB associations in the Galaxy and Magellanic Clouds (Conti 1992; Parker et al. 1992) demonstrates a range of IMF slopes γ (where $N(M) \propto M^\gamma$) from −2.0 to −3.1 with a typical value of −2.5, which we adopt as the IMF slope for NGC 5930's nuclear star forming region. In order to apply Leitherer's models, the ionizing luminosity must be estimated from the Hα luminosity. Assuming $T = 10^4$ K and that the gas is optically thick to Lyman continuum photons (case B), the number of ionizing photons emitted per second $Q(\mathrm{H}^0)$ and the Hα luminosity $L(\mathrm{H}\alpha)$ in ergs s^{-1} are related by

$$\frac{Q(\mathrm{H}^0)}{L(\mathrm{H}\alpha)} = \frac{\alpha_B}{\alpha_{\rm eff}(\mathrm{H}\alpha)} \frac{1}{h\nu_{\mathrm{H}\alpha}} = 7.3 \times 10^{11}, \qquad (2)$$

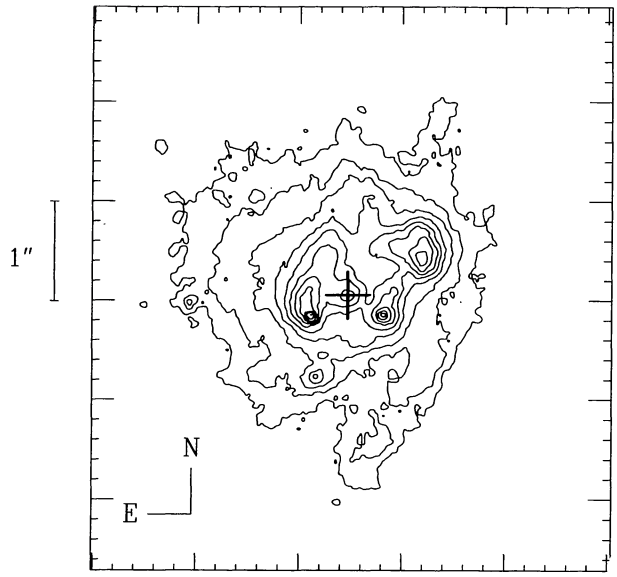

FIG. 2*a*

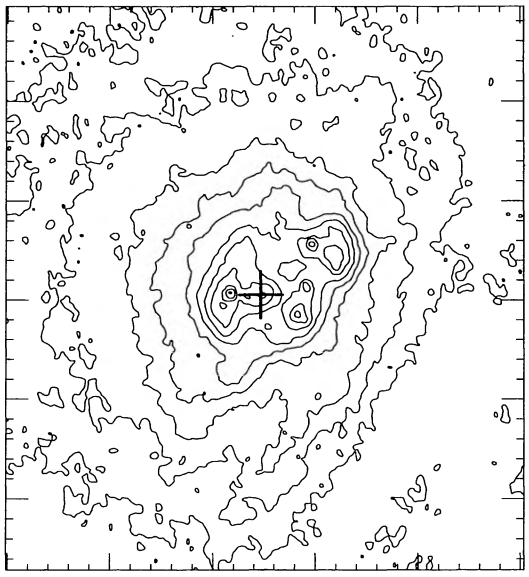

FIG. 2*b*

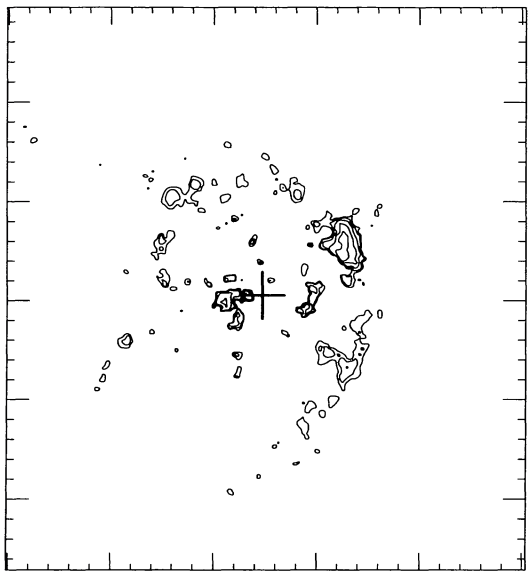

FIG. 2*c*

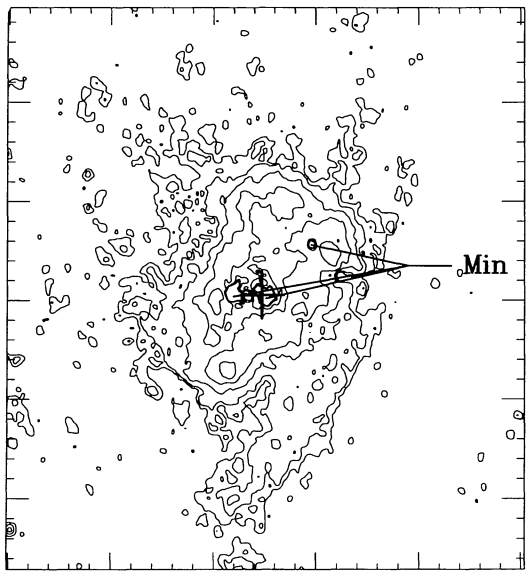

FIG. 2*d*

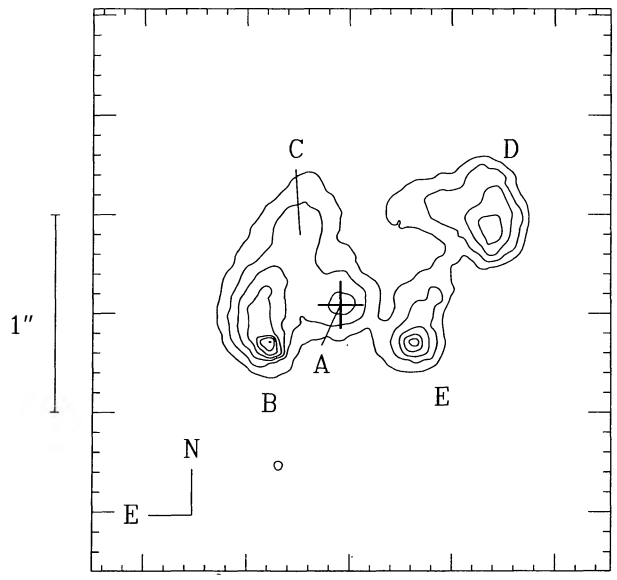

FIG. 2*e*

FIG. 2.—Contour plots of the deconvolved *HST* Planetary Camera images of the nuclear region of NGC 5930 showing the nuclear star forming region. The plots have resolution of 0″.1. The nucleus is adopted to be the centroid of the continuum isophotes outside $R = 2''$. This position (marked by a cross in Figs. 2–4) also corresponds to a peak in the continuum images. The brightest contour in plots (*a*)–(*d*) (which have identical scale and orientation) corresponds to the peak intensity; thus the brightest contour represents only 1 or 2 pixels. (*a*) The 5460 Å continuum image; contours range from 6.6×10^{-17} to 6.6×10^{-15} ergs cm^{-2} s^{-1} Å^{-1} arcsec^{-2} with an interval of 0.5 mag. (*b*) The 7160 Å continuum image; contours range from 5.1×10^{-17} to 5.1×10^{-15} ergs cm^{-2} s^{-1} Å^{-1} arcsec^{-2} with an interval of 0.5 mag. (*c*) The Hβ + [O III] image; contours range from 5.1×10^{-15} to 5.1×10^{-13} ergs cm^{-2} s^{-1} arcsec^{-2} with an interval of 1 mag. (*d*) The Hα + [N II] image; contours range from 3.7×10^{-15} to 3.7×10^{-13} ergs cm^{-2} s^{-1} arcsec^{-2} with an interval of 1 mag. The locations of minimum intensity inside the nuclear star forming region are indicated. (*e*) An expanded view of (*a*) showing the identification of the possible nuclear star clusters, the properties of which are given in Table 3.

TABLE 3

STAR CLUSTERS IN THE NUCLEAR REGION OF NGC 5930

STAR CLUSTER[a]	d[b]	V	M_V[c]	$(V-R)$	μ_0(V) (mag arcsec^{-2})	r_c (arcseconds)	r_c (h^{-1} pc)
A	0.″34	19.2	−13.0 (−16.8)	1.4	16.2	0.15	20
B	0.69	17.6	−14.6 (−18.4)	1.2	14.5	<0.05	<7
C	0.34	19.3	−12.9 (−16.7)	1.2	16.4	0.23	31
D	0.69	17.9	−14.3 (−18.1)	1.0	15.5	0.15	20
E	0.34	19.1	−13.1 (−16.9)	1.1	15.4	0.07	9
Nuclear region	2.58	15.9	−16.3 (−20.1)	1.2	...	...	...

[a] Star cluster identification from Fig. 2*e*.
[b] Aperture diameter (1″ = 135 h^{-1} pc).
[c] Absolute V magnitude of the individual star clusters for H_0 = 100 km s^{-1} Mpc^{-1} and no extinction correction, followed (in parentheses) by the absolute magnitude corrected for the best estimate of the gaseous extinction (A_V = 3.8 mag).

where α_B and $\alpha_{\rm eff}(\rm H\alpha)$ are hydrogen recombination coefficients, and $\nu_{\rm H\alpha}$ is the frequency of the Hα transition. Table 4 lists the estimated values of SFR and $R_{\rm SN}$ with their uncertainties, which reflect the possible range of IMF slopes found in OB associations (see above). Other uncertainties include the unknown star formation history and the uncertain extinction correction. Leitherer's (1990) models assume a constant SFR in a region with an age in excess of $\simeq 10^7$ yr, at which $Q(\rm H^0)$ becomes constant with time (see Leitherer's Fig. 6). The calculated SFR and $R_{\rm SN}$ will differ if the star formation in NGC 5930 has occurred in a recent burst.

An estimate of the supernova rate is also provided by the nonthermal radio luminosity when combined with a starburst model (e.g., Condon & Yin 1990). Table 5 lists the flux densities of the 4″ diameter nuclear radio source in NGC 5930 detected with the VLA (0.″4 beam at 6 cm) by Ulvestad & Wilson (1984). Possible mechanisms for generating the observed radio emission include thermal and nonthermal emission from the nuclear star forming region and nonthermal emission from relativistic electrons in the global magnetic field. In order to obtain the nonthermal radio luminosity, we must first estimate the emission from the other two components.

As discussed by Sramek & Weedman (1986), the luminosity of thermal radio emission, L_ν^T(1.46 GHz), from the nuclear star forming region at 20 cm can be estimated from $Q(\rm H^0)$ through

$$L_\nu^T(1.46\ \rm GHz) = 1.51 \times 10^{-26}\, Q(H^0)\,.$$

The flux density of thermal radio emission is found to be only $\simeq$2% of the total flux density observed at 1.46 GHz. Thus the observed radio emission is dominated by synchrotron radiation, as also indicated by the steep spectrum (Table 5).

The synchrotron emission from cosmic ray electrons in the global magnetic field of NGC 5930 can be roughly assessed by considering the typical intensity expected from the disk component in other disk galaxies (e.g., Condon 1992). Turner & Ho (1994) state that the typical brightness temperature of the disk at 6 cm is 0.2 K or less. This is a factor of ~230 below the sensitivity of the Ulvestad & Wilson map. Thus, both thermal radio emission from the H II regions and nonthermal emission from the disk are negligible contributors to the nuclear radio emission detected in NGC 5930. The conclusion that the radio emission is dominated by nonthermal emission from the star forming region is consistent with the observation that the radio source is elongated in P.A. = 156° (Ulvestad & Wilson 1984), similar to the major axis of the emission-line ring. Contributors to this nonthermal radio emission include supernovae, super-

TABLE 4

THE NUCLEAR STAR FORMING REGION IN NGC 5930

Quantity	Value
Aperture radius	2″
$L(\rm H\alpha + [N\ II])$	$1 \times 10^{40}\ h^{-2}$ ergs s^{-1}
[N II] λ6583/Hα[a]	0.64
$L(\rm H\alpha)$[b]	$7 \times 10^{40}\ h^{-2}$ ergs s^{-1}
$Q(H^0)$	$5 \times 10^{52}\ h^{-2}$ photons s^{-1}
SFR[c]	$0.07^{+0.09}_{-0.03}\ h^{-2}\ M_\odot$ yr^{-1}
$R_{\rm SN}$[c]	$(3^{+4}_{-2}) \times 10^{-3}\ h^{-2}$ yr^{-1}

[a] Keel et al. 1985.
[b] Corrected for $A_{\rm H\alpha}$ = 2.9 mag.
[c] Stellar mass range = 5–120 $M_\odot$.

TABLE 5

RADIO EMISSION FROM THE NUCLEAR STAR FORMING REGION IN NGC 5930

Quantity	Value
Radio source position (1950.0)[a]	$\alpha = 15^{\rm h}24^{\rm m}20^{\rm s}.77$, $\delta = +41°50'59''.4$
S_ν(4.88 GHz)[a]	12.0 ± 1.5 mJy
S_ν(1.46 GHz)[a]	39.0 ± 3.0 mJy
α[b]	0.98 ± 0.16
S_ν^T(1.46 GHz)[c]	0.79 mJy
$L_\nu^{\rm NT}$(1.46 GHz)[d]	$3.5 \times 10^{28}\ h^{-2}$ ergs s^{-1} Hz^{-1}
$R_{\rm SN}$[e]	$3.9 \times 10^{-2}\ h^{-2}$ yr^{-1}

[a] Ulvestad & Wilson 1984; estimated error in position is ±0.″1.
[b] $S_\nu \propto \nu^{-\alpha}$.
[c] Flux density of thermal radio emission, calculated from the Hα flux (§ 4.1).
[d] Nonthermal radio luminosity.
[e] Supernova rate estimated from eq. (3).

nova remnants (SNRs), and electrons which have diffused out of the SNRs.

Condon & Yin (1990) derive an empirical relationship between the nonthermal radio luminosity from a starburst region and the supernova rate:

$$L_\nu^{\rm NT} = 1.3 \times 10^{30} \left(\frac{\nu}{1\ {\rm GHz}}\right)^{-\alpha} R_{\rm SN}\,, \qquad (3)$$

where $L_\nu^{\rm NT}$ is in ergs s^{-1} Hz^{-1} and $R_{\rm SN}$ is in yr^{-1}. For NGC 5930, $L_\nu^{\rm NT}(1.46\ {\rm GHz}) = 3.5 \times 10^{28}\ h^{-2}$ ergs s^{-1} Hz^{-1}, so $R_{\rm SN} = 3.9 \times 10^{-2}\ h^{-2}$ yr^{-1}. This rate is a factor of $\sim$13 higher than the rate derived above from the Hα luminosity. Possible explanations for this discrepancy include: (1) the extinction correction applied to the observed Hα flux may have been underestimated; (2) the radio emission may include a contribution from Type I supernova remnants (i.e., those with progenitor star masses $<8\ M_\odot$), although Condon & Yin regarded such a contribution as insignificant; (3) some of the nonthermal radio emission might originate from a weak or hidden active nucleus; and (4) the steady state model adopted for the star formation rate might be incorrect.

4.2. *Possible Formation Scenarios for the Nuclear Star Forming Region*

The enhanced nuclear star formation rate in NGC 5930 may be related to its interaction with NGC 5929. Published simulations of galaxy encounters include both mergers and flybys. Since NGC 5929 and NGC 5930 have not (yet) merged, simulations of flybys (e.g., Mihos, Richstone, & Bothun 1992) may be more relevant here than simulations of mergers (e.g., Barnes & Hernquist 1991). Mihos et al.'s models include the flyby of two disk galaxies on parabolic orbits covering four possible orbital geometries (prograde-prograde, prograde-retrograde, retrograde-retrograde, and highly inclined). In the prograde-prograde encounter, both disk galaxies are rotating in the plane of the orbit of the galaxy pair and in the same rotational sense as their orbital motion (see Mihos et al. for a definition of the other three orbital geometries). Of the four orbital geometries modeled by these authors, only the prograde-prograde and prograde-retrograde flybys resulted in a significant increase in SFR and a concentration of gas at the nucleus (i.e., the features observed in NGC 5930).

The ring-like morphology of the ionized gas in NGC 5930 may reflect a nonaxisymmetric gravitational potential. Such potentials can cause dynamical resonances involving the orbital speed Ω, the pattern speed Ω_p, and the epicyclic frequency κ (e.g., Binney & Tremaine 1987). In a survey of spiral galaxies, Buta (1986) identified specific resonances with the rings and pseudorings that occur frequently in spiral galaxies. Additional modeling (e.g., Schwarz 1984; Combes & Gerin 1985) has demonstrated that nuclear rings with enhanced star formation can form at the inner Lindblad resonance due to the concentration of interstellar gas there. The ringlike morphology of the ionized gas in NGC 5930 could thus be related to an inner Lindblad resonance. In this interpretation, the turnover in the rotation curve should be near the ring (e.g., Kormendy & Norman 1979). The small radius ($\approx$135 h^{-1} pc) of the nuclear ring in NGC 5930 thus implies that the gravitating mass is strongly concentrated toward the nucleus.

5. SUMMARY

We have analyzed images of the spiral galaxy NGC 5930 obtained with the Planetary Camera aboard *HST* covering the emission lines of [O III] $\lambda\lambda$4959, 5007 + Hβ and Hα + [N II] $\lambda\lambda$6548, 6583 and their adjacent continua. The results can be summarized as follows:

1. Five bright continuum knots are located within the central $\simeq$1.″5 (200 h^{-1} pc). The central knot coincides with the centroid of the isophotes at larger radii, so we have adopted this position as the nucleus. These knots represent either star clusters or a smooth stellar distribution affected by patchy obscuration. Since the darker areas around the knots are not significantly redder than the stellar population outside the nuclear region ($R \geq 2''$), and since Hα + [N II] emission is detected between the knots, the interpretation of the knots as star clusters is favored.

2. An elliptical ring of low-excitation gas with dimensions 2.″4 $\times$ 1.″6 (320 $h^{-1} \times$ 220 h^{-1} pc) is associated with the star clusters. The emission-line ring has an axial ratio $b/a \approx 0.67$ and major axis position angle $\approx$140°, close to the values for the outer disk, suggesting that the ring lies in the plane of the disk. Since this gas is of low-excitation and there is no evidence for an active galactic nucleus in NGC 5930, this giant H II region is presumably photoionized by hot stars, which may reside in the nuclear star clusters.

3. The Hα luminosity of the nuclear giant H II region, when corrected for an uncertain estimate of the extinction, is similar to that of well-studied giant H II regions in nearby galaxies (e.g., M101) and implies a star formation rate (SFR) for 5–120 $M_\odot$ stars $\approx$ 0.07 $h^{-2}\ M_\odot$ yr^{-1} and a rate of supernova events from massive progenitor stars of $\approx 3 \times 10^{-3}\ h^{-2}$ yr^{-1}. These estimates are somewhat uncertain (see § 4).

4. A possible model which may account for the formation of the nuclear star forming ring involves the concentration of gas at or near the inner Lindblad resonance(s), with subsequent star formation. The small radius of the ring (135 h^{-1} pc) then implies that the inner mass distribution is strongly concentrated toward the nucleus.

A detailed investigation of the stellar population and the determination of the location of the inferred inner Lindblad radii would require high spatial resolution spectrophotometry of the nuclear region.

We thank L. Bergeron for assistance with the data reduction, and we acknowledge useful discussions with S. Baum, C. Leitherer, C. Mihos, J. Mulchaey, C. O'Dea, R. Pogge, T. Storchi-Bergmann, and N. Walborn. We thank M. Mateo for obtaining broad-band images of NGC 5930 with the Michigan Dartmouth MIT 2.4 m telescope to verify the presence of the bar. S. Westphal assisted with the plates. Partial support for this work was provided by NASA through grant number GO-3724 from the Space Telescope Science Institute, which is operated by AURA, Inc., under NASA contract NAS5-26555. Additional support was provided by NASA grants NAGW-2689 and NAGW-3268.

REFERENCES

Allen, C. W. 1973, Astrophysical Quantities (London: Athlone)
Argyle, R. W., & Clements, E. D. 1990, Observatory, 110, 93
Arp, H. C. 1966, ApJS, 14, 1
Barnes, J. E., & Hernquist, L. 1991, ApJ, 370, L65
Benedict, G. F., et al. 1993, AJ, 105, 1369
Binney, J., & Tremaine, S. 1987, Galactic Dynamics (Princeton: Princeton Univ. Press)
Bower, G. A., Wilson, A. S., Mulchaey, J. S., Miley, G. K., Heckman, T. M., & Krolik, J. H. 1994, AJ, 107, 1686
Burstein, D., & Heiles, C. 1984, ApJS, 54, 33
Buta, R. 1986, ApJS, 61, 609
Buta, R., & Crocker, D. A. 1993, AJ, 105, 1344
Combes, F., & Gerin, M. 1985, A&A, 150, 327
Condon, J. J. 1992, ARA&A, 30, 575
Condon, J. J., & Yin, Q. F. 1990, ApJ, 357, 97
Conti, P. S. 1992, in IAU Symp. 149, The Stellar Populations of Galaxies, ed. B. Barbuy & A. Renzini (Dordrecht: Kluwer), 93
de Vaucouleurs, G., de Vaucouleurs, A., Corwin, H. G., Buta, R. J., Paturel, G., & Foque, P. 1991, Third Reference Catalog of Bright Galaxies (New York: Springer)
Grillmair, C. J., Faber, S. M., Lauer, T. R., Baum, W. A., Lynds, C. R., O'Neill, E. J., Jr., & Shaya, E. J. 1994, AJ, 108, 102
Keel, W. C. 1985, Nature, 318, 43
Keel, W. C., Kennicutt, R. C., Jr., van der Hulst, J. M., & Hummel, E. 1985, AJ, 90, 708
Kennicutt, R. C., Jr. 1984, ApJ, 287, 116
Kennicutt, R. C., Jr., Keel, W. C., van der Hulst, J. M., Hummel, E., & Roettiger, K. A. 1987, AJ, 93, 1011
Kormendy, J., & Norman, C. A. 1979, ApJ, 233, 539
Lasker, B. M., et al. 1990, AJ, 99, 2019
Leitherer, C. 1990, ApJS, 73, 1
Lucy, L. B. 1974, AJ, 79, 745
MacKenty, J. W. et al. 1992, *Hubble Space Telescope* Wide Field and Planetary Camera Instrument Handbook Version 3.0 (Baltimore: Space Telescope Science Institute)
Mihos, J. C., & Hernquist, L. 1994, ApJ, 431, L9
Mihos, J. C., Richstone, D. O., & Bothun, G. D. 1992, ApJ, 400, 153
Mulchaey, J. S., Wilson, A. S., Bower, G. A., Heckman, T. M., Krolik, J. H., & Miley, G. K. 1994, ApJ, 433, 625
Noguchi, M. 1988, A&A, 203, 259
Osterbrock, D. E. 1989, Astrophysics of Gaseous Nebulae and Active Galactic Nuclei (Mill Valley, CA: University Science Books)
Parker, J. W., Garmany, C. D., Massey, P., & Walborn, N. R. 1992, AJ, 103, 1205
Savage, B. D., & Mathis, J. S. 1979, ARA&A, 17, 73
Schwarz, M. P. 1984, MNRAS, 209, 93
Sramek, R. A., & Weedman, D. W. 1986, ApJ, 302, 640
Turner, J. L., & Ho, P. T. P. 1994, ApJ, 421, 122
Ulvestad, J. S., & Wilson, A. S. 1984, ApJ, 285, 439
Wakamatsu, K., & Nishida, M. T. 1988, ApJ, 325, 596